A Comparative Numerical Simulation Study of Turbulent Non-premixed $CO/H_2/N_2$ Syngas Jet Flames

M.T. Lewandowski[*, 1, 2], J. Pozorski[1]

[1]Institute of Fluid-Flow Machinery, Polish Academy of Sciences, Gdańsk
[2]Gdańsk University of Technology, Conjoint Doctoral School GUT and IFFM PAS

Abstract

In the present work, numerical simulations of turbulent non-premixed syngas flame have been performed in Reynolds-Averaged Naver-Stokes turbulence approach using four turbulence-chemistry interaction models. To this aim, we used assumed beta PDF approach, Steady Laminar Flamelet model, Eddy Dissipation Concept and Partially Stirred Reactor model. Numerical results are compared and analysed with respect to two experiments from the TNF Workshop data sets. The most accurate predictions were obtained with the Partially Stirred Reactor model in OpenFOAM. Finally, we present a simulation of an industrial combustion chamber designed for low-calorific gas burning.

1. Introduction

Numerical computation of turbulent reactive flows is a challenging task due to the multi-scale character of the phenomena, both in space and time. There are two main problems: complex chemistry and turbulence itself. In industrial applications with complex geometry there occur supplementary phenomena such as phase change, wall interaction, thermo-acoustic effects, instabilities etc. Low calorific fuels like syngas obtained from biomass waste are of interest due to the current European energy strategy. Utilization of such fuel in efficient and environmentally friendly way involves additional difficulties.

The key difficulty in mathematical modelling of the turbulent combustion phenomena is the source term in the species transport equation. Reaction rate is based on the Arrhenius law which is highly non-linear, and it is not easy to express it as a function of mean values. Expanding the mean reaction rate as a Taylor series of the temperature fluctuation leads to various difficulties and is not commonly used [1]. Therefore existing models are based on physical analysis, comparing chemical and turbulent time scales and, according to Veynante and Vervisch [2], most of them can be classified as one-point statistics, geometrical analysis or turbulent mixing approach. We can observe multiplicity of such approaches used in the literature, yet there is no ready answer which one gives best results.

Lysenko et al. [3] used Eddy Dissipation Concept (EDC) implemented with URANS formulation with *OpenFOAM* toolbox in order to simulate the flame Sandia CHNa and the Sydney bluff-body stabilized flame HM1E. They compared their results with β-pdf method and Steady Laminar Flamelet model. Marzouk and Huckaby [4] used modified version of the *reactingFoam* solver using Partially Stirred Reactor Model (PaSR), distributed with *OpenFOAM* version 1.5. They studied eight finite-rate chemistry kinetic mechanisms for CO/H_2 combustion in CHNa configuration. Both groups used modified $C_{\varepsilon 1}$ constant in the $k-\varepsilon$ turbulence model. Cuoci et al. [5] did similar simulations with *Ansys Fluent* code. Kim and Kim [6] developed Eulerian particle flamelet model proposed by Barths et al. [7] simulating both flames, CHNa and CHNb, using $k-\varepsilon$ model with Pope's correction. Giacomazzi et al. [8] performed calculations of this flame using Large Eddy Simulation.

The aim of the present work is to analyse and compare behaviour of the four different turbulence-chemistry interaction models in the same flow modelling conditions. Analysis of the Sandia CHNb flame (referred also as a syngas flame) in that purpose has been done. The acquired knowledge gives us information what one may expect from the used model and chemical mechanism in industrial applications.

2. Theory and modelling

2.1. Turbulent flow

In order to deal with the problem of turbulent reactive flow, one has to solve the system of closed equations of motion, energy conservation and species transport equations. In the present work the Navier-Stokes equations are subject to Reynolds decomposition and Favre averaging, resulting in the following form [1]:

$$\frac{\partial \bar{\rho}}{\partial t}+\frac{\partial}{\partial x_j}\left(\bar{\rho}\tilde{u}_j\right)=0\,, \tag{1}$$

$$\frac{\partial}{\partial t}\left(\bar{\rho}\tilde{u}_i\right)+\frac{\partial}{\partial x_j}\left(\bar{\rho}\tilde{u}_i\tilde{u}_j\right)=-\frac{\partial \bar{p}}{\partial x_i}+\frac{\partial}{\partial x_j}\left(\bar{\tau}_{ij}-\bar{\rho}\widetilde{u_i''u_j''}\right)+\bar{\rho}\tilde{f}_i\,, \tag{2}$$

$$\frac{\partial}{\partial t}\left(\bar{\rho}\tilde{Y}_k\right)+\frac{\partial}{\partial x_j}\left(\bar{\rho}\tilde{Y}_k\tilde{u}_j\right)=\frac{\partial}{\partial x_j}\left(\bar{\rho}D_k\frac{\partial \tilde{Y}_k}{\partial x_j}-\bar{\rho}\widetilde{Y_k''u_j''}\right)+\bar{R}_k\,, \tag{3}$$

$$\frac{\partial}{\partial t}\left(\bar{\rho}\tilde{h}\right)+\frac{\partial}{\partial x_j}\left(\bar{\rho}\tilde{h}\tilde{u}_j\right)=\frac{\partial}{\partial x_j}\left(\bar{\rho}\alpha\frac{\partial \tilde{h}}{\partial x_j}-\bar{\rho}\widetilde{h''u_j''}\right)+\bar{S}_h\,. \tag{4}$$

The closure for the turbulent fluxes can be obtained by statistical modelling based on turbulent viscosity. The Reynolds stresses can be written as:

* Corresponding author: michal.lewandowski@imp.gda.pl

$$-\bar{\rho}\,\widetilde{u_i''u_j''} = \mu_t\left(\frac{\partial\tilde{u}_i}{\partial x_j}+\frac{\partial\tilde{u}_j}{\partial x_i}\right)-\frac{2}{3}\left(\bar{\rho}k+\mu_t\frac{\partial\tilde{u}_l}{\partial x_l}\right)\delta_{ij}\,. \quad (5)$$

The turbulent fluxes of scalars are written in terms of gradient model:

$$-\widetilde{Y_k''u_j''} = D_t\frac{\partial\tilde{Y}_k}{\partial x_j}=\frac{\nu_t}{Sc_t}\frac{\partial\tilde{Y}_k}{\partial x_j}\,, \quad (6)$$

$$-\widetilde{h''u_j''} = \alpha_t\frac{\partial\tilde{h}}{\partial x_j}=\frac{\nu_t}{\mathrm{Pr}_t}\frac{\partial\tilde{h}}{\partial x_j}\,, \quad (7)$$

where Sc_t and Pr_t are turbulence Schmidt and Prandtl numbers respectively. Turbulent dynamic viscosity is calculated as:

$$\mu_t=\bar{\rho}\nu_t=C_\mu\bar{\rho}\frac{\tilde{k}^2}{\tilde{\varepsilon}}\,. \quad (8)$$

The turbulent kinetic energy k and its dissipation rate ε are obtained with a two equation $k-\varepsilon$ turbulence model.

2.2. Turbulence-chemistry interaction models

2.2.1. Assumed Probability Density Function

One of the approaches for turbulence-chemistry interaction is a model with assumed probability density function using mixture fraction as a passive scalar. The idea lies behind defining a mixture fraction ξ in the way that it is linked with instantaneous mass fractions Y_k in the relation $Y_k(\xi)$ and takes values 0 in the oxidizer stream inlet and 1 in fuel inlet:

$$\xi=\frac{Z_k-Z_{k2}}{Z_{k1}-Z_{k2}}\,. \quad (9)$$

A commonly used definition is the one proposed by Bilger or the one using elemental mass fractions [1, 9]. This approach is valid for infinitely fast, irreversible chemistry and the Lewis number equal to one. Then, the mean species mass fractions are obtained from [1]:

$$\bar{\rho}\tilde{Y}_k=\int_0^1 Y_k(\xi)\rho(\xi)p(\xi)d\xi\,, \quad (10)$$

where $p(\xi)$ is the probability density function which is often assumed as a β function, parameterized by the mean mixture fraction and its second moment (mixture fraction variance). Then instead of N species mass fraction transport equations only those for ξ and ξ'' are resolved.

2.2.2. Steady Laminar Flamelet

Steady Laminar Flamelet model assumes that the structure of a turbulent flame can be reconstructed by one-dimensional laminar flames embedded in a turbulent flow [10]. In order to do that, a so-called flamelet equation needs to be solved for a laminar flame (analogous for the temperature):

$$\rho\frac{\partial Y_k}{\partial t}=\frac{1}{2}\rho\chi\frac{\partial^2 Y_k}{\partial\xi^2}+R_i\,, \quad (11)$$

where $\chi=2D(\nabla\xi)^2$ is a scalar dissipation rate, and its stoichiometric value may be used as a parameter for correct representation of the turbulent flow. Local derivative is neglected in a steady state approach. Then functions $Y_k(\xi,\chi_{st})$ are stored in "flamelet libraries" and used to evaluate mean values of mass fractions [1]:

$$\bar{\rho}\tilde{Y}_k=\int_0^{+\infty}\int_0^1\rho Y_k(\xi,\chi_{st})p(\xi,\chi_{st})d\xi d\chi_{st}\,. \quad (12)$$

2.2.3. Eddy Dissipation Concept

Eddy Dissipation concept is based on turbulent mixing and its main assumption is that the combustion occurs where turbulence energy dissipation takes place – in so-called fine structures [3, 11, 12]. A control volume is divided into fine structures and the surroundings. Mass exchange between the structures is considered giving as a result expression for a mean source term in eq. (3):

$$\bar{R}_k=-\frac{\bar{\rho}\dot{m}\eta}{1-\gamma^*\eta}\left(\tilde{Y}_k-Y_k^*\right), \quad (13)$$

where only a fraction of fine structures react $0\le\eta\le1$ and ratio between their mass to the total mass is postulated to be:

$$\gamma^*=\left(\frac{3C_{D2}}{4C_{D1}^2}\right)^{1/2}\left(\frac{\nu\varepsilon}{k^2}\right)^{1/2}. \quad (14)$$

In the previous version of the model, this expression was in the power of ¾ [3, 11], which may be still implemented in some codes. One can choose to use Eq. (13) to import detailed chemical mechanism and solve additional Ordinary Differential Equations (ODE) for perfectly stirred reactor (PSR) or simplify the problem to local extinction or fast chemistry approach [12].

2.2.4. Partially Stirred Reactor

Another method for turbulence-chemistry interaction recalls a detailed chemistry approach of EDC is Partially Stirred Reactor (PaSR) [13]. Here each computational cell is also split into two zones: reacting and non-reacting. A reacting zone is a homogenous composition which can be treated as PSR [14]. The mean reaction rate for the species k is given by the following expression [4, 14]:

$$\bar{R}_k=\kappa_k R_k\,, \quad (15)$$

where R_k is the reaction rate of the species according to the used kinetic mechanism. The reactive fractions κ_k depend on both the chemical time scale τ_{ch} and the micro-mixing time scale τ_m [14]:

$$\kappa_k=\frac{\tau_{ch}}{\tau_m+\tau_{ch}}\,, \quad (16)$$

where:

$$\tau_m=C_{mix}\sqrt{\frac{\mu_{eff}}{\rho\varepsilon}}\,. \quad (17)$$

3. Case description

The analysed test case comes from the Turbulent Non-premixed Flames (TNF) Workshop database of simple jet flow and flames of various fuels. It corresponds to the $CO/H_2/N_2$ jet flame investigated by Barlow [15, 16] at Sandia and velocity measurements

were conducted by Flury [17] at ETH Zurich. They studied two such flames with the same fuel composition (40% CO, 30% H_2 and 30% N_2 by volume) and $\mathrm{Re} = 16700$ based on fuel jet velocity and nozzle diameter, different for the two flames. For our simulations, we chose the flame CHNb characterized by a nozzle diameter d=7.72 mm and velocity of the fuel stream U_{jet}=45 m/s. The coflow air velocity was U_{air}=0.7 m/s and the stoichiometric mixture fraction for this flame was equal to 0.295.

4. Numerical simulations

The calculations were carried out using commercial code *Ansys Fluent* and open source package *OpenFOAM* version 2.3.0, both based on finite volume method. We assumed that the flame is in axi-symmetric geometry, which allowed us to use 2D computational mesh. However, because of differences in geometry managing in the two codes, we were forced to use two different grids. For the *Ansys Fluent* a simple 2D mesh (Fig. 1) with axis of rotation was generated in *ICEM CFD*, whereas for *OpenFOAM* a wedge type, axi-symmetric geometry with *blockMesh* utility was created. Mesh size tests allowed us to use 9949 cells size grid in the first case (19.43d and 108.8d in radial and axial direction respectively) and 7550 cells in the second (19.43d and 115.28d in radial and axial directions respectively).

In the *Ansys Fluent* calculations, SIMPLEC algorithm was used for coupling pressure and velocity fields with PRESTO! pressure interpolation method. Second-order upwind schemes were adopted for spatial discretization. In *OpenFOAM*, the PIMPLE algorithm and second-order Gaussian integration schemes were used for space. The *reactingFoam* solver is designed for transient problems but, since we were looking for a steady-state solution, we used a first-order implicit Euler method for the time derivative. Semi-implicit Bulirsch-Stoer (SIBS) solver was used for integrating stiff ordinary differential equations of perfectly stirred reactor.

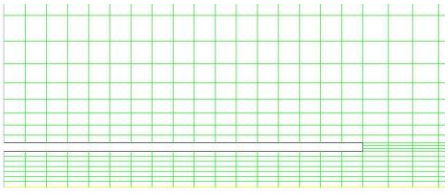

Fig. 1. A view of the near inlet part of the computational grid for flame CHNb in Ansys Fluent.

5. Results

In Fig. 2, the temperature profiles along axis of the CH_4 and Syngas flames are presented in the configuration of Sandia flame D [18], which was studied in our previous work [19]. Assumed β pdf method was used. The red line represents numerical results for methane combustion as in Sandia flame D but with no pilot stream. This configuration is characterized by $\mathrm{Re} = 22400$ with a fuel jet velocity U_{jet}=49.6 m/s, a nozzle diameter equal to 7.2 mm and a coflow air velocity U_{air}=0.9 m/s. The fuel composition of 25% CH_4 diluted with 75% air by volume was still above the upper flammability limit, so that the flame behaved as in the non-premixed regime. The green line represents the second case where we tried to compare methane with syngas in the same composition as in the CHNb flame. Not surprisingly, the obtained result did not differ much from the original Sandia flame D, as the lower heating value for such fuel compositions was similar (9.225 and 7.819 MJ/kg, respectively). Therefore the blue line represents such a jet with a composition of only 25% of fuel (15% CO and 10% H_2) and 75% N2. The air as a dilution gas could not be used in this case as it would compose a flammable mixture. Having the same volumetric fuel composition in both cases, one can see that the syngas flame is cooler and shorter than the methane flame.

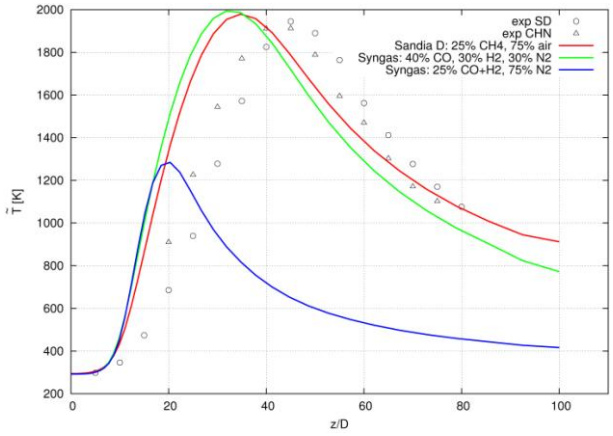

Fig. 2. Experimental data for the mean temperature profiles along the axis for the Sandia flame D and CHNb (circles and triangles, respectively). Color lines represent numerical results for the geometry of flame D with different fuel composition.

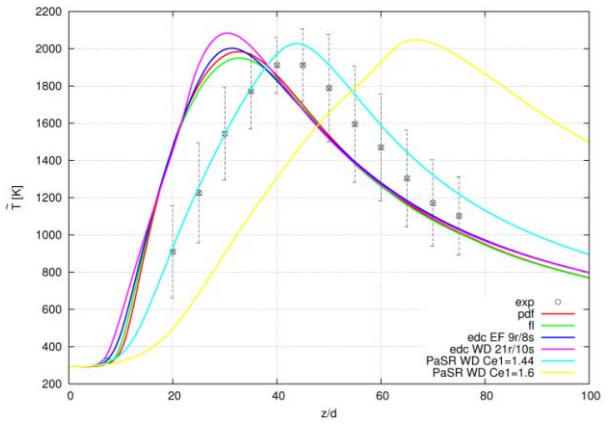

Fig. 3. The mean temperature along the axis of CHNb flame for four different approaches in six configurations. Assumed β pdf method (red line), steady laminar flamelet model (green line), eddy dissipation concept with Edelman and Fortune (blue line) and with Westbrook and Dryer chemical mechanism (purple line), Partialy Stirred Reactor model with Westbrook and Dryer chemical mechanism and $C_{\varepsilon 1}$ constant set to 1.44 (turquoise line) and 1.6 (yellow line). The rms fluctuations plotted as uncertainty bars.

Fig. 3 displays the mean temperature profile for the four studied models. One can be surprised with very similar distribution for the β pdf, SLF and EDC model, yet other scalar distributions behave differently. Worth noticing here is a change in the temperature peak value when changing chemical mechanism in EDC from (9 reactions and 8 species) Edelman and Fortune (taken from [4]) to (21 reactions and 9 species) Westbrook and Dryer kinetics [20]. In the second case the maximum temperature value is much higher than it is expected even though the used chemical mechanism was more complex. However the same kinetics (Westbrook and Dryer) adopted in Partially Stirred Reactor model in *OpenFOAM* code gave very satisfactory results. Temperature is overestimated on the downstream side of the jet and in its maximum value, due to the fact that radiation is not included in this simulation. The yellow line represents results obtained with the same model but a changed constant $C_{\varepsilon 1}$ from 1.44 to 1.6 in the $k-\varepsilon$ turbulence model, as in [3, 4]. Serious deterioration of the results is observed by that. Marzouk and Huckaby [4] did not check Westbrook and Dryer mechanism with standard constant and Lysenko et al. [3] artificially improved β pdf model results. However they refer to have a better flow solution with this corrected constant. There are many other references in the literature with modified value of the constant for round jets (see for instance [21]). However in our simulations it is not clear whether results obtained with 1.44 or 1.6 values of $C_{\varepsilon 1}$ are better (Fig. 4), but as long as we use standard values for all other combustion models we will stay with 1.44.

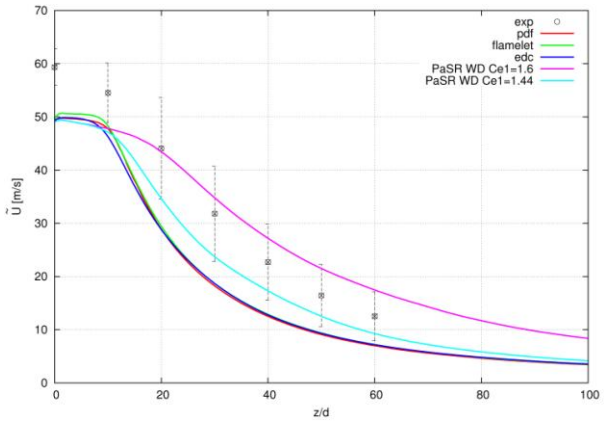

Fig. 4. Velocity magnitude values along the axis of the jet for the four combustion models: β pdf, SLF, EDC (*Ansys Fluent*) and PaSR (*OpenFOAM*) with standard $C_{\varepsilon 1}$ constant and for PaSR with modified constant value.

In Fig. 5, chosen radial distributions of the mean temperature are presented, where only PaSR model reconstitute character of the experimental data. In the other cross sections PaSR model shows better behaviour as well.

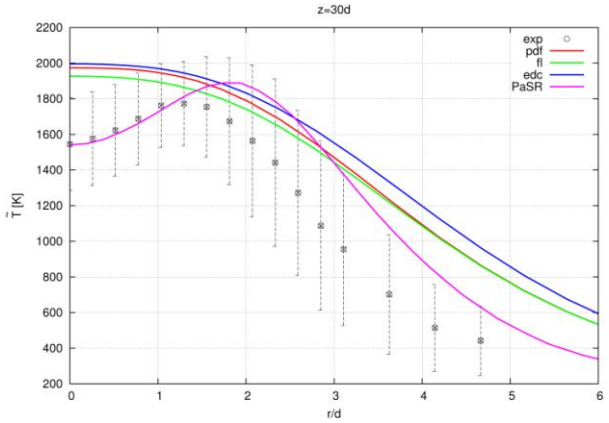

Fig. 5. Radial distribution of the mean temperature for β pdf (red line), SLF (green line), EDC (Edelman and Fortune chemical mechanism, blue line) and PaSR (Westbrook and Drayer chemical mechanism, purple line) at axial distance $z = 30d$.

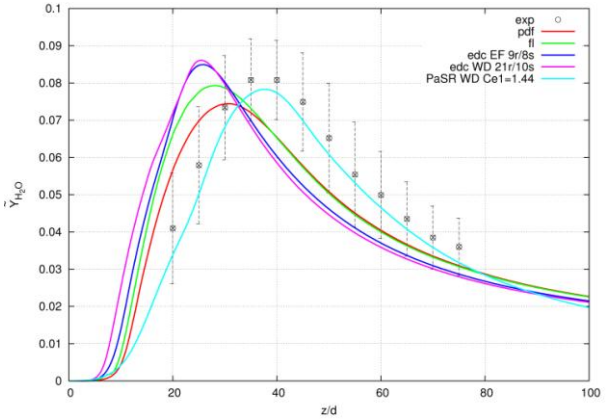

Fig. 6. Mass fraction of water vapor along the axis.

For the three models used in *Ansys Fluent* more differences can be observed in the predictions of water vapor presented in Fig. 6. There were two chemical mechanisms implemented to eddy dissipation concept as well. However much better distribution was obtained again with PaSR. Moreover, this model is the only one that predicted the OH radical distribution correctly, as shown in Fig. 7. Significant discrepancies between numerical results obtained with EDC model and experiments raise some concerns about its implementation or incorporated chemical mechanism. We expected to obtain better performance of this mixing model in comparison to the latter ones.

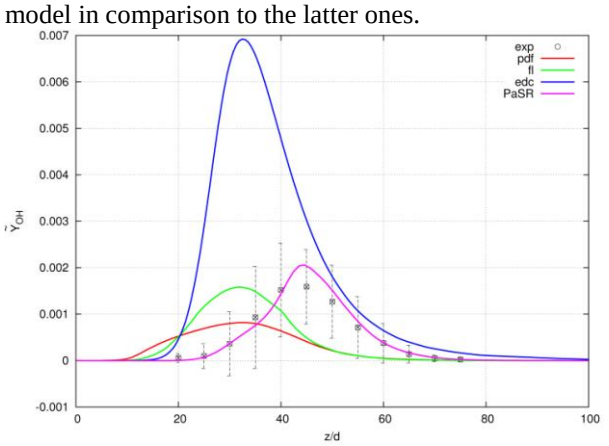

Fig. 7. Mass fraction of a OH radical along the axis.

The PaSR model proved to reproduce the flame structure the most properly but we encountered some problems with its execution. We started to run calculations beginning with irreversible Arrhenius type reactions, gradually switching one by one to the reversible type. Otherwise we received an error or obtained unphysical flame lift-off (Fig. 8). Moreover, the occurrence of the lift-off depended on the order of the operation. We managed to switch on to reversible type all the reactions in Westbrook and Dryer mechanism instead of the following three reactions: $OH \leftrightarrow O + H$, $H_2 \leftrightarrow H + H$ and $H_2O \leftrightarrow H + OH$. The first two gave lift-off and with the last one we could not start the calculations at all.

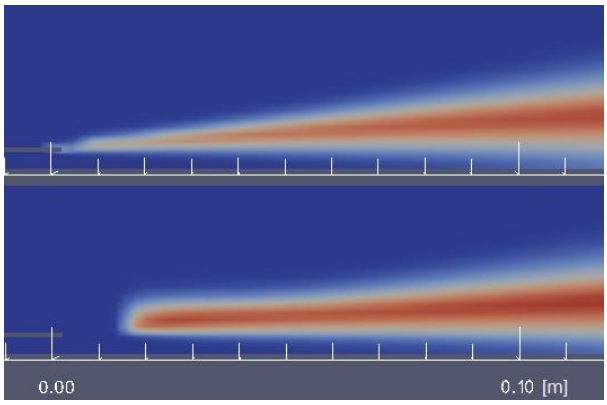

Fig. 8. Contours of the mean temperature during conditions when the flame is attached to the jet wall (top picture) and when there is a lift off (bottom picture).

Finally, we performed a numerical simulation of CHN fuel combustion in the industrial combustion chamber designed for burning low calorific gas from gasification of waste biomass. It is 5.5 m high and has a radius of 1.3 m and approximately 30 m^3 of volume. The geometry was created by [22]. We generated computational mesh (2.1M cell) in *snappyHexMesh* utility and imported it to *Ansys Fluent*. At this stage we used β pdf approach as the chemistry-turbulence interaction method, $k-\varepsilon$ turbulence model and spherical harmonics P1 approximation for radiation modelling. The simulation was performed as a steady state.

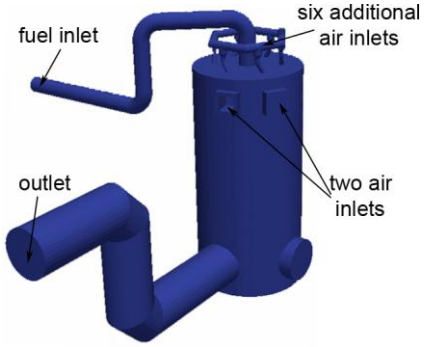

Fig. 9. Geometry of combustion chamber based on the installed unit in gasification plant in Olsztyn, Poland [22, 23].

The boundary conditions were chosen so that a rough qualitative comparison with [22] case 2B may be done. We adjusted the CHN fuel mass flow rate to 0.2899 kg/s, which corresponds to the power equal to 2.674 MW calculated on the basis of lower heating value of syngas used in [22]. As it was presented in Fig. 2, we should not expect significant differences of flame structure using such an analogy. The operating air-fuel ratio was 3.45 resulting in a lean equivalence ratio $\phi = 0.867$. The temperature of syngas leaving the gasifier has a significant contribution to its total energy content, and we set its value to 1000 K, whereas the air temperature was 300 K.

In Fig. 10, contours of the static temperature in the two cross sections of the chambers are shown from three different points of view. The highest calculated temperature is about 1880 K and the flame length is two thirds of the chamber's height. The temperature field of the hot flue gases in the outlet cross-section is presented in Fig. 11. A strong temperature gradient directed towards the left side is visible, which is caused by a flame tilt due to the side air streams. All the fuel was consumed in the chamber, only trace amounts of CO and H_2 can be found in the outlet.

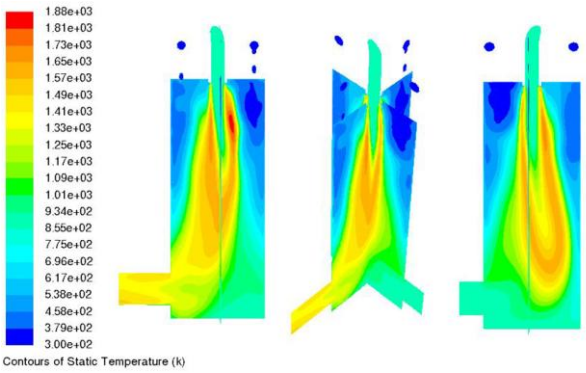

Fig. 10. Contours of a static temperature for the two cross sections of the combustion chamber.

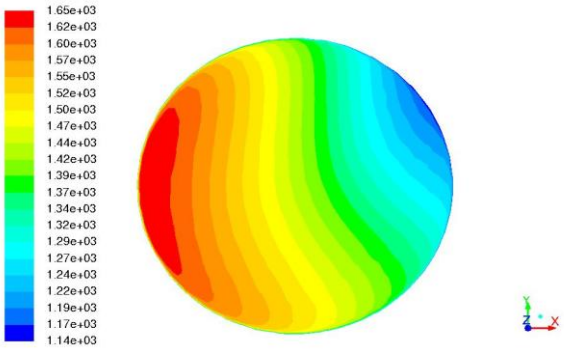

Fig. 11. Contours of a static temperature at the outlet of the combustion chamber.

6. Perspectives

In the future we will correct small differences between the numerical setup of the cases and recalculate them. We do not expect major changes due to that effect, however it will be more accurate for the

comparative study. Nevertheless, the PaSR model proved to be the most accurate in all the cases in contrast to other models. However we need to point out the higher computational cost of the mixing type models (PaSR and EDC).

We predict some other improvements as well. The inlet velocity needs to be adjusted in all the cases to reconstruct experimental axial velocity distribution. Radiation in the PaSR calculations should be included and mesh, at least in the inlet region, needs to be refined. In this area, we encountered numerical problems as it was predicted in [15].

In the case of the combustion chamber, we performed a steady state computation, therefore no flame oscillations reported in Kwiatkowski et al. [22] were observed in our simulation. Yet, these results give a good general overview of the combustion in the chamber and may be used as initial conditions for the next simulation. In the case of combustion chamber, where wall treatment is important, the Shear Stress Transport (SST) $k-\omega$ turbulence model will be probably more appropriate as well as Discrete Ordinates method for radiation. As it was shown in the case of Sandia flame CHNb, we expect to obtain better results with Partially Stirred Reactor model, implemented in *OpenFOAM*.

Acknowledgements

Part of this work was supported by the research task financed within the framework of the Strategic Research and Development Programme entitled 'Advanced Technologies for Energy Generation' carried by The National Centre for Research and Development and electric power holding company ENERGA SA in Poland. Research Task No. 4 "Development of Integrated Technology of Fuels and Energy from Biomass, Agricultural Waste and Other".

References

[1] T. Poinsot, D. Veynante, Theoretical and Numerlical Combustion, Third Edition, Aquaprint, Bordeaux, 2012.

[2] D. Veynante, L. Vervisch, Prog. Energy Comb. Sci., 28 (2002) 193-266.

[3] D. A. Lysenko, I. S. Ertesvåg, K. J. Rian, Flow Turbul. Combust. 93 (2014) 577-605.

[4] O. A. Marzouk, E.D. Huckaby, Eng. Appl. Comp. Fluid. 4 (2010) 331–356.

[5] A. Cuoci, A Frassoldati, G. Buzzi Ferraris, T. Faravelli, E. Ranzi, Int. J. Hydrogen Energ. 32 (2007) 3486-3500.

[6] S. K. Kim, Y. Kim, Combustion and Flame 154 (2008) 232-247.

[7] H. Barths, N. Peters, N. Brehm, A. Mack, M. Pfitzner, V. Smiljanowski, Proc. Combust. Inst. 27 (1998) 1841-1847.

[8] E. Giacomazzi, F.R. Picchia, N. Arcidiacono, D. Cecere, F. Donato, B. Favini, Combust. Theor. Model. 12 (2008) 1125–1152.

[9] Libby P.A., Williams F.A. Topics in Applied Physics vol. 44 Turbulent Reacting Flows, Springer-Verlag, 1980.

[10] N. Peters, Turbulent Combustion, Cambridge University Press, 2000.

[11] B. Magnussen, The Eddy Dissipation Concept: A Bridge between Science and Technology, ECCOMAS Thematic Conference on Computational Combustion, Lisbon, 2005.

[12] B. Lilleberg, D. Christ, I. S. Ertesvåg, K. Rian, R. Kneer, Flow Turbul. Combust. 91 (2013) 319-346.

[13] V. I. Golovitchec, J. Chomiak, Numerical Modeling of High Temperature Air "Flameless" Combustion, The 4th International Symposium on High Temperature Air Combustion and Gasification, Rome, 2001.

[14] G. D'Errico, D. Ettorre, T. Lucchini, Comparison of Combustion and Pollutant Emission Models for Dl Diesel Engines, International Conference on Internal Combustion Engines, Naples, 2007.

[15] R.S. Barlow, G.J. Fiechtner, C.D. Cartner, J.Y. Chen, Combust. Flame 120 (2000) 549-569.

[16] R.S. Barlow et al., Sandia/ETH-Zurich CO/H2/N2 Flame Data – Release 1.1, Sandia National Laboratories, 2002.

[17] M. Flury, Experimentelle Analyse der Mischungstruktur in turbulenten nicht vorgemischten Flammen, Ph.D. Thesis, ETH Zurich, 1998.

[18] R.S. Barlow, J. H. Frank, Proc. Combust. Inst. 27 (1998) 1087-1095.

[19] M.T. Lewandowski, J. Pozorski in M. Szewczyk (Eds), Applications of Thermodynamic Analysis in Description of Physical Phenomena In Energy Devices (in Polish), OWPRz, Rzeszów 2014.

[20] C. K. Westbrook, F. L. Dryer, Combust. Sci. Technol. 27 (1981) 31-43.

[21] F.C. Christo, B.B. Dally, Combust. Flame 142 (2005) 117-129.

[22] K. Kwiatkowski, M. Dudyński, K. Bajer, Flow Turbul. Combust. 91 (2013) 749–772.

[23] K. Kwiatkowski, K. Bajer, K. Wędołowski, Arch. Mech. 64 (2012) 511-527.